Available online at www.sciencedirect.com
ScienceDirect
Polymer 47 (2006) 7145–7152
polymer
www.elsevier.com/locate/polymer

High-performance polypropylene film prepared from reactor powders having different characteristics

Hiroki Uehara [a,*], Tomomi Hirao [b], Takeshi Yamanobe [a], Tadashi Komoto [a], Yuzo Yamamoto [b]

[a] Department of Chemistry, Gunma University, 1-5-1 Tenjin-cho, Kiryu, Gunma 376-8515, Japan
[b] Department of Biological and Chemical Engineering, Gunma University, 1-5-1 Tenjin-cho, Kiryu, Gunma 376-8515, Japan

Received 30 January 2006; received in revised form 27 June 2006; accepted 2 July 2006
Available online 17 August 2006

Abstract

Ultra-high molecular weight isotactic polypropylene (UHMW-iPP) reactor powders have been successfully ultra drawn below melting temperature (T_m) by a combination of calendar rolling and tensile drawing techniques. Two UHMW-iPP reactor powders having different MWs were synthesized by using the same Ziegler–Natta catalyst system at 70 °C in hexane. The resultant tensile properties increased with increasing draw ratio, due to orientation–crystallization during tensile draw, which was indicated by DSC and WAXD measurements. The film drawn under optimum conditions exhibited the maximum tensile modulus of ~25 GPa, independent of sample MW, corresponding to 70% of the ultimate modulus of iPP crystal. However, the higher maximum tensile strength of ~1.0 GPa was achieved for the reactor powder having the higher MW, which is three times as high as those of commercial high-strength iPP tapes. Such a fact that high performances have been achieved by processing from reactor powder state below T_m implies that crystallization with less entanglement occurs during polymerization. When drawability and resultant properties were compared among different iPP reactor powders prepared under different conditions, it was clarified that they were predominantly affected by not only MW but also by the reactor powder morphology, especially surface smoothness.

Keywords: Isotactic-polypropylene; Reactor powder; Drawing

1. Introduction

It is known that the less-entangled reactor powder morphologies are formed during polymerization for highly crystalline polymers, including polyethylene (PE) [1–5] and polytetrafluoroethylene (PTFE) [6,7]. Especially, the reactor powder synthesized by slurry process is thought to have a single-crystal like morphology because the crystallization during polymerization proceeds in the solvent. However, such a unique reactor powder characteristics is easily lost once molten and usual spherulite structure is retained on recrystallization [3]. Therefore, reactor powder processing, including the compression molding and subsequent coextrusion and tensile drawings all below the T_m, has been tried in 1980s [8–15]. The feature of this drawing technique lies in utilizing the superior characteristics of as-polymerized state for reactor powder without any melt processing such as pelletizing or melt-extrusion. It has been reported that the high-performance films having 70% of crystal modulus are obtainable for PE [8–12] and PTFE [14,15] by using this processing technique.

Isotactic polypropylene (iPP) is one of the polyolefins and has the higher T_m and toughness than PE. Therefore, iPP is widely used as food packaging and automobile parts. Today, one of fifth of total plastic production in industries is occupied by iPP production in the world [16]. Here, it has been reported that the ultra-high molecular weight iPP (UHMW-iPP) is ultra-drawable from its solution-crystallized film, which is similar to UHMW-PE. The resultant tensile modulus achieved 95% of the theoretical modulus (35 GPa [17]) of iPP crystal [18]. Thus, there is a possibility that the high-performance iPP film can be prepared by reactor powder processing of UHMW-iPP, as well as UHMW-PE. The morphologies of iPP reactor powder

* Corresponding author. Tel.: +81 277 30 1332; fax: +81 277 30 1333.
E-mail address: uehara@chem.gunma-u.ac.jp (H. Uehara).

0032-3861/$ - see front matter © 2006 Elsevier Ltd. All rights reserved.
doi:10.1016/j.polymer.2006.07.065

have been studied [19–24], however, there is no report on the preparation of the high-performance film from iPP reactor powder although the iPP reactor powder is synthesized using Ziegler–Natta catalyst system, which is almost the same for the synthesis of PE reactor powder having higher ductility. This might be attributed to the poor adhesion between reactor powder particles of iPP, compared to that of PE, when the initial film preparation was made by simple compression molding below T_m. In this study, we applied calendar rolling to improve the adhesion between iPP reactor powder particles even below their T_m. A combination of shear stress on such rolling process and tensile force on subsequent drawing enables a direct preparation of the high-performance film from iPP reactor powder.

2. Experimental section

2.1. Samples

Two UHMW-iPPs (PP-1 and PP-2) used in this work were prepared by slurry-polymerization at 70 °C in heptane with the same Ziegler–Natta catalyst system. As a compared sample, the commercial iPP reactor powder (PP-3) having a conventional MW was purchased from Aldrich Chemical Company. The weight average MW (M_w), tacticity, average particle size, T_m and crystallinity were summarized in Table 1. Tacticities of the sample powders were defined by isotactic pentad fractions (*rrrr*) estimated from ^{13}C NMR spectroscopy measured by TOSOH Analysis and Research Center in Yokkaichi, Japan. For these tacticity analyses, the sample powder was dissolved in dichlorobenzene at 150 °C.

2.2. Film preparation

The direct film preparations from above reactor powders were made using roll-processing machine with the parallel arrangement of two polished stainless rolls having 100 mm diameter and 150 mm width. The distance between the two rolls is adjusted to the desired film thickness, then, reactor powder was put on the hollow gap made by such parallel arrangement of two rolls. A continuous rolling at 2 rpm manufactured the molded films. The temperature of these two rolls (T_{roll}) was isothermally kept in the range of 150–170 °C.

2.3. Drawing

The drawing specimens were cut into a strip with 50 mm length and 5 mm width along the rolling direction. These ribbons were tensile drawn at constant drawing temperatures (T_{draw}) of 125–165 °C and at a constant crosshead speed, corresponding to the initial strain rate of 1 min^{-1}, in an Orientec Tensilon tensile tester RTC-1325A equipped with an air oven. The draw ratio (DR) was determined from the separation of ink marks preprinted on the surface of samples. In the case that the second-stage tensile drawing was also made after the first-stage drawing, the total DR (DR_t) was defined by DR_t = (first-stage DR) × (second-stage DR).

Table 1
Characterization of iPP reactor powders used in this study

Sample	M_w (10^5)	Size (μm)	Tacticity[a]	T_m (°C)[b]	χ_c (%)[b]
PP-1	15.0	150	95.1	163	43
PP-2	23.0	150	98.7	167	44
PP-3	8.5	150	91.7	161	46

[a] Evaluated by isotactic pentad fraction (*rrrr*) estimated from ^{13}C NMR spectroscopy measured in dichlorobenzene at 150 °C.
[b] Estimated from DSC measurements.

2.4. Soxhlet extraction

The reactor powder surface of PP-1 was modified by soxhlet extraction using hot heptane for 72 h. After such solvent extraction procedure, the sample powder was dried in vacuum.

2.5. Measurements

A Perkin–Elmer Pyris 1 was used to analyze the melting behavior. The DSC heating scan was followed up to 200 °C at an H.R. of 10 °C/min under nitrogen gas flow. Calibration of DSC characteristics, including melting temperature and heat of fusion, was made by using an indium and tin standards. The sample T_m was evaluated by a peak position of the endotherm. The fraction crystallinities were calculated from the heat of fusion (ΔH_f). The enthalpy value of 210 J/g was used as that of the perfect crystals of iPP [25].

Wide-angle X-ray diffraction (WAXD) pattern of the oriented films were recorded on a Fuji Film imaging plate BAS-SR. Cu $K\alpha$ radiation monochromatized with a Ni-filter was generated at 40 kV and 120 mA by a Rigaku RU-200B rotating anode X-ray generator. The incident beam was radiated perpendicular to the film surface. The recorded imaging plate pattern was read out using Rigaku R-AXIS DS3.

The tensile modulus and strength on the machine direction were measured at room temperature and at strain rates of $1 \times 10^{-3}\ s^{-1}$ and $1 \times 10^{-2}\ s^{-1}$, respectively. The modulus was determined from the slope of the stress/strain curve at low strain (<0.1%).

Scanning electron microscope (SEM) observations of untreated and treated reactor powders were made using a JEOL JSM-T20 operated at 5 kV. The powder surface was coated by Au with 8 nm using JEOL ion spatter JFC-1000. Optical microscopic (OM) observation for the prepared film was made using an Olympus BX-50 microscope. The photographs were taken perpendicular to the film thickness direction with 100× magnification.

3. Results and discussions

3.1. Direct film manufacturing

As the first trial, PP-1 reactor powder having an M_w of 1.5×10^6 was used for a direct film processing and subsequent property development by tensile drawing. On the processing from reactor powder, an effective processing is usually enabled just below the sample melting of the reactor powder

for UHMW-PE [8–12]. Therefore, the melting behavior of PP-1 reactor powder was analyzed by DSC measurement, as shown in Fig. 1. Below the T_m of 163 °C of PP-1 reactor powder, three T_{roll}s of 150 °C, 155 °C, and 160 °C were selected as represented by the dotted lines in Fig. 1. Another T_{roll} of 165 °C, which is a little beyond the sample T_m, was also selected for a comparison.

Next, in order to evaluate the adhesion between reactor powder particles, the tensile tests of these prepared films were made at room temperature. At a T_{roll} of 150 °C, the sponge-like film was output from the gap between two parallel rolls, but its tensile test was ineffective. Table 2 represents the yield stress, breaking stress and breaking strain for these roll-processed films. The film prepared at a T_{roll} of 155 °C was immediately broken with no necking phenomenon as soon as the tensile test was initiated. In contrast, the stress–strain curve of the film prepared at a T_{roll} of 160 °C exhibited the apparent necking at the early stage of draw. Both yielding and breaking stresses of this film were the highest among all films prepared in this study, which means that the most desirable adhesion between reactor powder particles was obtained at a T_{roll} of 160 °C. When the T_{roll} was increased to 165 °C, these stress values decrease significantly, but the strain at break increases extremely. Such stress–strain characteristics are very similar to those of the melt-processed film, as shown in Table 2. Finally, the T_{roll} of 160 °C is selected as the optimum processing condition, where the film processing proceeds in the solid state and an enough adhesion between reactor powder particles is attained.

The morphology and structure of the film direct-rolled from PP-1 reactor powder at an optimum T_{roll} of 160 °C are shown in Fig. 2. In case of the Fig. 2a, the prepared film was put on a black sheet for clear recognition of the film appearance. It can be seen that the film is homogeneously transparent, meaning the better adhesion between reactor powder particles. The thickness of the film was constant along the rolling direction, but different from 100 μm at the left and right edges to 140 μm at the center of the film. The higher magnification reveals the

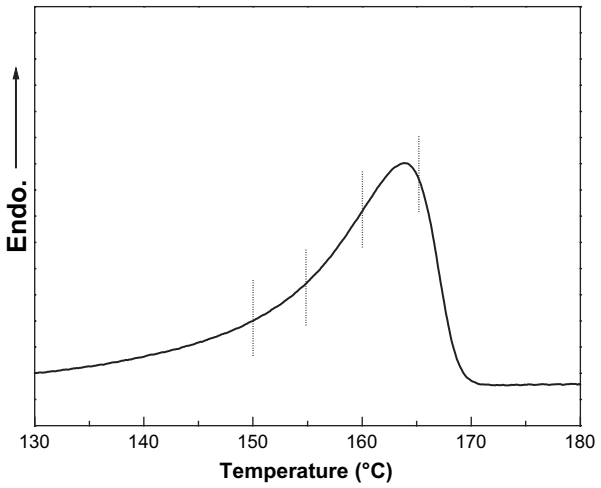

Fig. 1. DSC melting thermograms of PP-1 reactor powder recorded at a heating rate of 10 °C/min. The dotted lines indicate the T_{roll}s examined.

Table 2
Tensile properties of PP-1 films prepared at T_{roll} = 155, 160, 165 °C and compression-molded at 210 °C

T_{roll} (°C)	Yield stress (MPa)	Stress at break (MPa)	Strain at break (%)
155	26.5	14.0	–
160	34.9	33.2	41
165	22.5	14.1	189
MP film[a]	23.1	18.8	271

[a] Melt-pressed film was prepared by compression molding of PP-1 reactor powder at 210 °C for 30 min.

power boundaries, as shown in the Fig. 2b. Thus, it is expectable that the reactor powder state with less entanglement is kept within the direct-rolled film. The WAXD pattern (Fig. 2c) exhibits the chain orientations both parallel and perpendicular to the rolling direction, which can be confirmed from the arc-shaped (110) reflections on the equator and meridian. Such dual chain orientations are often observed for tensile drawing of iPP with a partial melting [26].

3.2. Property developments by tensile drawing

For property development of the above films prepared from UHMW-iPP reactor powder, their tensile drawings were further made under various T_{draw}s. Fig. 3 compares the stress–strain curves recorded during tensile drawing at different T_{draw}s of 130–160 °C. Until a T_{draw} of 145 °C, the maximum achievable DR (DR_{max}) increased with increasing T_{draw}, however, decreased beyond this T_{draw}.

Such T_{draw} effect on the drawability is attributed to a combination of the activation of the molecular motion by increasing the T_{draw} below 145 °C and subsequent relaxation of the oriented molecules during drawing above 150 °C.

Next, the mechanical properties of these drawn films were compared. Fig. 4 shows the tensile modulus measured at room temperature as a function of DR for the films prepared at various T_{draw}s. The tensile modulus increases with increasing DR for all the T_{draw}s. At a T_{draw} of 145 °C, the maximum achievable modulus (E_{max}) of 19 ± 1 GPa was obtained at DR_{max}. This modulus value corresponds to 60% of the theoretical modulus of iPP crystal [17]. This achieving percentage is a little lower than 70% for the ultra-drawn film prepared from UHMW-PE reactor powder [8,11], meaning a possibility of the further development of the tensile modulus for iPP reactor powder processing. Therefore, the subsequent second-stage tensile drawing was applied for these first-stage tensile-drawn films.

As shown in Fig. 3, the optimum T_{draw} was 145 °C for the first-stage drawing; thus, the film drawn at this T_{draw} up to DR 10, where the necking was fully transmitted across both chucks of the specimen, was used as the starting material for the second-stage drawing. Here, the two T_{draw}s at the first- and second-stage drawings were distinguished by the superscript such as T^1_{draw} and T^2_{draw}. Fig. 5 compares the stress–strain curves recorded during drawing from a DR 10 film at different T^2_{draw}s of 150–160 °C. It is found that the DR_{max} is obtained at a T^2_{draw} of 155 °C. Therefore, this temperature

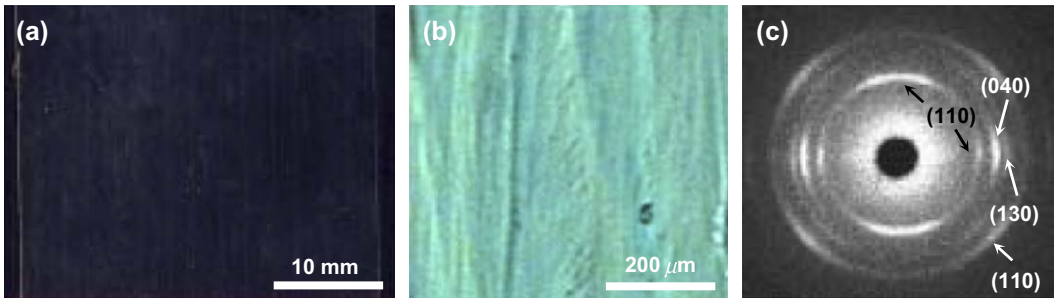

Fig. 2. The photograph (a), OM image (b) and WAXD pattern (c) of the film direct-rolled from PP-1 reactor powder at an optimum T_{roll} of 160 °C. Rolling direction is always vertical.

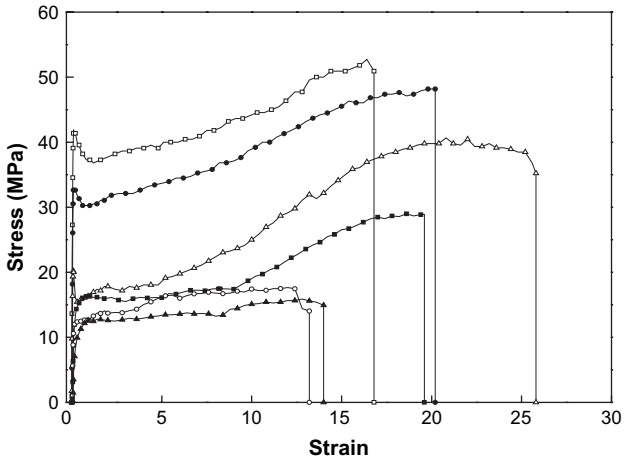

Fig. 3. Stress–strain curves recorded on drawing for the PP-1 film prepared at a T_{roll} of 160 °C. Draws were made at different T_{draw}s of 130 °C (□), 140 °C (●), 145 °C (△), 150 °C (■), 155 °C (○) and 160 °C (▲) under a constant crosshead speed giving an initial strain rate of 1 min^{-1}.

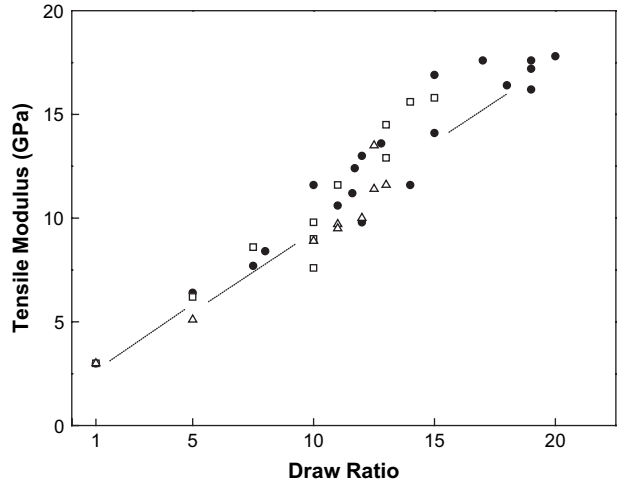

Fig. 4. Resultant tensile modulus vs. DR for the PP-1 films prepared at a T_{roll} of 160 °C subsequently tensile-drawn at different T_{draw}s of 135 °C (□), 145 °C (●) and 155 °C (△).

was determined as the optimum T_{draw} for the second-stage drawing.

The tensile modulus of the thus prepared two-stage drawn film was compared to that of the first-stage drawn film, as shown in Fig. 6. For both drawn films, the tensile modulus linearly increases with increasing DR. E_{max} for the second-stage drawing is higher than that for the first-stage drawing, due to the higher DR_{max} for the former, achieving to 25 ± 1 GPa at a $DR_{t,max}$ of 28. This modulus value corresponds to 70% of the theoretical modulus of the iPP crystal. Similarly, the tensile strength was also compared between the first- and second-stage drawn films, as shown in Fig. 7. The higher tensile strength was also obtained for the second-stage drawing, resulting in the maximum tensile strength (σ_{max}) of 0.7 ± 0.1 GPa at the same $DR_{t,max}$ of 28.

In order to discuss the structural change during these drawings, the DSC and WAXD measurements were carried out for the initial roll-processed film and the subsequently drawn films. Fig. 8 shows the plots of the crystallinities (χ_c) estimated from the DSC endotherms as a function of DR. The χ_c increases with increasing DR, reaching to the $\chi_c = 71\%$ at a $DR_{t,max}$ of 28. This χ_c value is well coincident with the achievable percentage of the sample modulus (70% compared to the theoretical one). The molecular orientations within the films were also evaluated by WAXD measurements, as shown in Fig. 9. For all films, only the reflections ascribed to the monoclinic lattice, which is the most stable crystalline form of iPP, were observed. Even for a lower DR 10 film, the

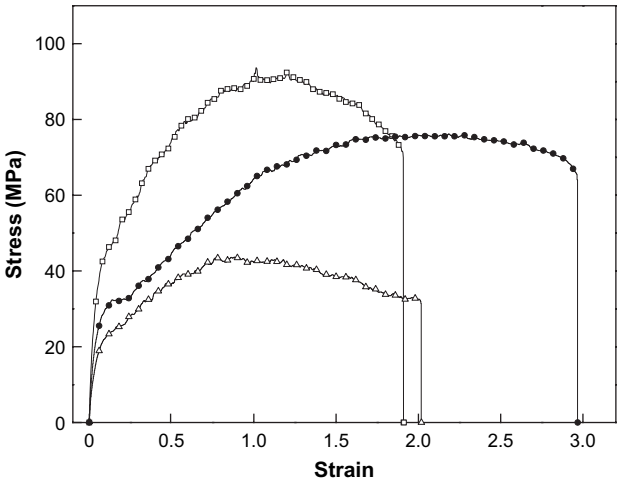

Fig. 5. Effect of T_{draw} on the stress–strain curves for second-stage tensile drawing from the film first-stage drawn up to DR 10. The second-stage draws were made at different T^2_{draw}s of 150 °C (□), 155 °C (●) and 160 °C (△).

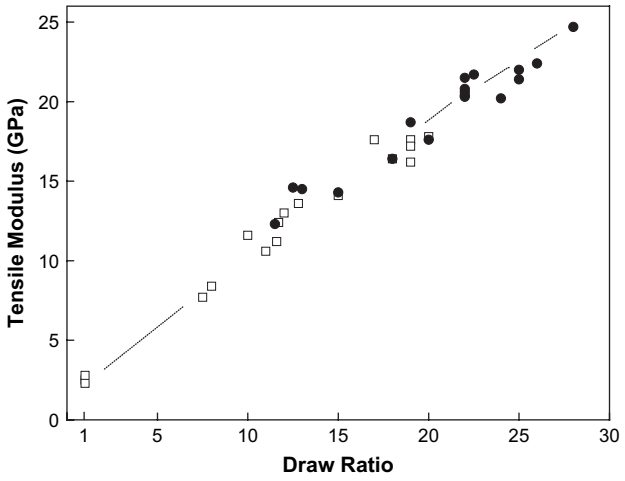

Fig. 6. Comparison of resultant tensile modulus obtained by first-stage (□) and second-stage draws (●). First- and second-stage draws were made at $T^1_{draw} = 145\ ^\circ C$ and $T^2_{draw} = 155\ ^\circ C$, respectively.

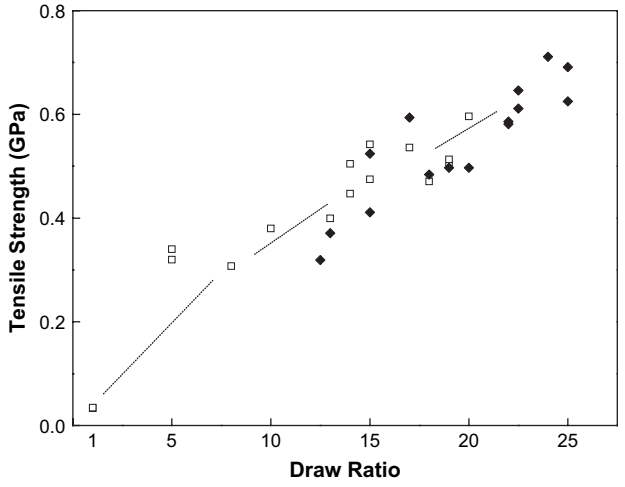

Fig. 7. Comparison of resultant tensile strength obtained by first-stage (□) and second-stage draws (◆). First- and second-stage draws were made at $T^1_{draw} = 145\ ^\circ C$ and $T^2_{draw} = 155\ ^\circ C$, respectively.

(*hk*0) reflections appear on the equator. These reflections concentrate as the spots with increasing DR. These results indicate that the molecular chains highly orient along the draw axis by tensile drawing. A combination of DSC and WAXD results reveals that the origin of tensile property developments (see Figs. 6 and 7) is ascribed to the oriented crystallization during tensile drawing.

3.3. Effect of powder morphology on resultant film properties

As described above, UHMW-iPP reactor powder can be successfully processed into the high-performance films, as well as UHMW-PE reactor powders. This implies that the higher crystalline state with less entanglement is formed during polymerization of UHMW-iPP reactor powder. Therefore, the various UHMW-iPP reactor powders were prepared under

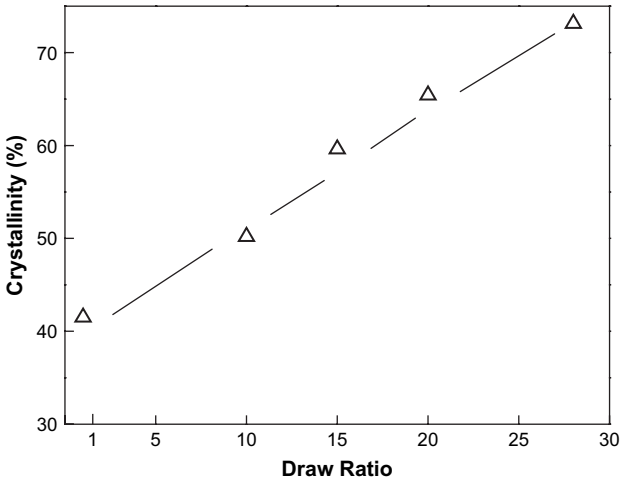

Fig. 8. Changes in the sample crystallinity with DR for the PP-1 films processed under optimum conditions.

different polymerization conditions and their drawability and resultant properties were compared.

Fig. 10 compares the sets of SEM images of the reactor powders of PP-1, which is examined above, and PP-2 having the higher M_w of 2.3×10^6. A commercial reactor powder PP-3, having a conventional M_w of 8.5×10^5, was used as a compared sample. The PP-1 reactor powder (Fig. 10a) has a relatively smooth surface. In contrast, the commercial PP-3 reactor powder (Fig. 10c) exhibits the rough surface morphology. Indeed, the film processing and subsequent drawing were examined for this PP-3 reactor powder, but the $DR_{t,max}$ was restricted at 18; thus, the lower E_{max} of ~19 GPa and σ_{max} of ~0.5 GPa were obtained, as shown in Table 3. Considering that the M_w of this PP-3 is lower than that of PP-1, both the reactor powder surface and sample MW give large influences on the resultant film properties.

In order to distinguish these different effects, the powder sample having a comparable M_w but different surface morphology was prepared by soxhlet extraction. Fig. 10d shows the SEM image obtained of PP-1 powder after soxhlet extraction by hot heptane for 72 h. Powder surface was smooth before this treatment (see Fig. 10a), but becomes rough after this treatment (Fig. 10d). When the treated PP-1 was used, the $DR_{t,max}$ was 21 and the resultant properties were E_{max} of 20 ± 1 GPa and σ_{max} of 0.5 ± 0.1 GPa, as shown in Table 3. These values are lower than those of the original reactor powder ($E_{max} = \sim 25$ GPa, $\sigma_{max} = \sim 0.7$ GPa). Namely, the reactor powder having the smooth surface gives the higher resultant properties for the roll-processing and subsequent tensile drawing examined in this study.

The above information indicates that both smooth surface and higher MW are necessary for the further property development. Therefore, the reactor powder PP-2 having the higher M_w of 2.3×10^6 was prepared using the same catalyst system as for the preparation of PP-1 reactor powder having the smooth surface morphology. As expected, the flatness of the PP-2 reactor powder was comparable to that of PP-1 reactor powder (see Fig. 9b). However, the T_m of PP-2 was 4 °C

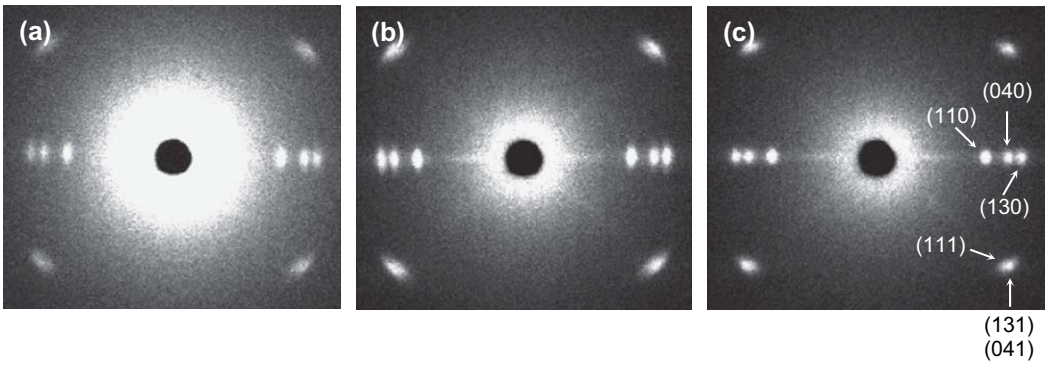

Fig. 9. WAXD patterns of drawn PP-1 films. (a) DR = 10, (b) $DR_t = 15$ and (c) $DR_{t,max} = 28$. Draw direction is vertical.

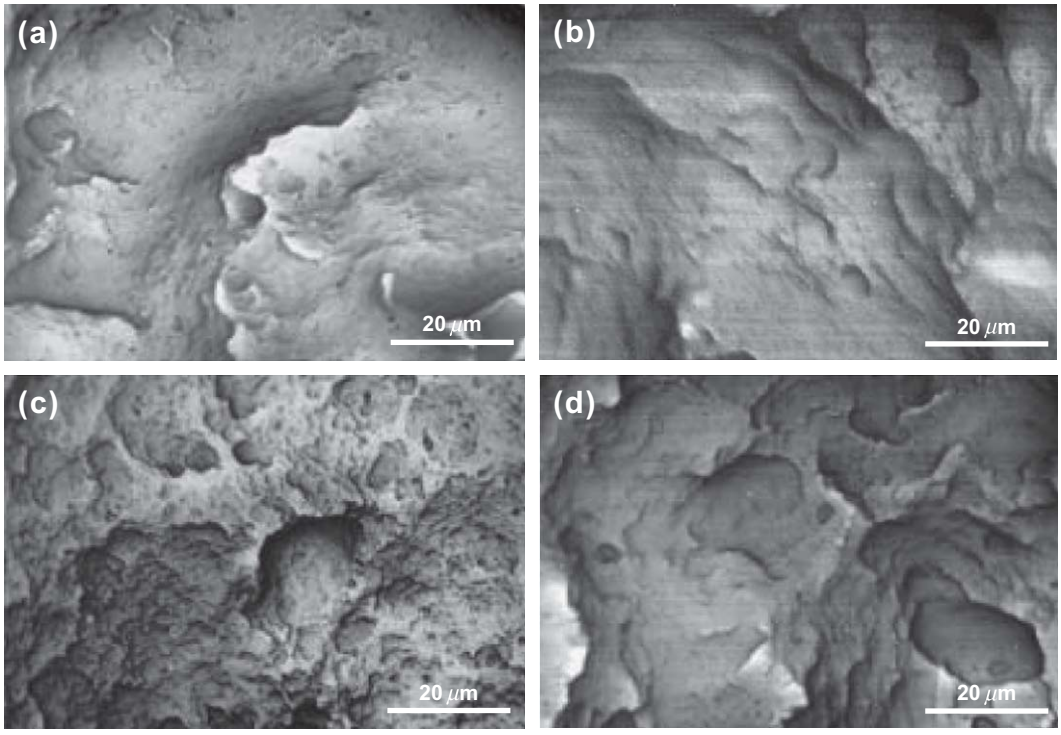

Fig. 10. SEM images of the reactor powders of PP-1 (a), PP-2 (b) and PP-3 (c) used in this study. For comparison, the image obtained after soxhlet extraction treatment of PP-1 powder is also included (d).

higher than that of PP-1, as shown in Table 1. Therefore, its optimum T_{roll} was newly determined. Table 4 summarizes the yielding stress, breaking stress and breaking strain estimated from the stress–strain curves recorded at room temperature for the roll-processed films prepared from PP-2 reactor powder at different T_{roll}s of 160–170 °C. Both maximum values in yielding and breaking stresses were obtained for the films prepared at a T_{roll} of 165 °C. Thus, this temperature was determined as the optimum T_{roll} for PP-2 reactor powder.

Since the T_{roll} was changed, the optimum T_{draw} was also examined again. Fig. 11 shows the effects of T_{draw} on the stress–strain curves of PP-2 films prepared at a T_{roll} of 165 °C. The T_{draw} giving the $DR_{t,max}$ was 145 °C, which is coincident with the optimum T_{draw} for the first-stage drawing of PP-1 (see Fig. 3). Therefore, the T^2_{draw} for second-stage drawing of PP-2 was also set up at the same optimum $T^2_{draw} = 155$ °C for PP-1. Under such new T_{draw} combination, the two-stage drawing was carried out for PP-2 reactor powder film. The resultant E_{max} of 25 ± 1 GPa and σ_{max} of 1.0 ± 0.1 GPa were obtained at a $DR_{t,max}$ of 28, as shown in Table 5. This E_{max} value is comparable to that of PP-1 reactor powder, indicating the similar level of the molecular orientation and crystallinity, due to the coincident drawability ($DR_{t,max}$). On the other hand, it is known that the tensile strength is significantly influenced

Table 3
Maximum draw ratio ($DR_{t,max}$), tensile modulus (E_{max}) and strength (σ_{max}) for the films prepared from UHMW-iPP reactor powders

Sample	$DR_{t,max}$	E_{max} (GPa)	σ_{max} (GPa)
PP-1	28	25 ± 1	0.7 ± 0.1
PP-3	18	19 ± 1	0.5 ± 0.1
PP-1 (treated)	21	20 ± 1	0.5 ± 0.1

Table 4
Tensile properties of PP-2 films prepared at $T_{roll} = 160-170$ °C and compression-molded at 210 °C

T_{roll} (°C)	Yield stress (MPa)	Stress at break (MPa)	Strain at break (%)
160	–	46.1	52
165	48.2	46.7	316
170	42.7	32.3	215
MP film[a]	31.8	29.3	480

[a] Melt-pressed film was prepared by compression molding of PP-2 reactor powder at 210 °C for 30 min.

by the sample M_w, thus the higher value was obtained for PP-2 reactor powder.

These results suggest that the dominant factors for resultant properties are the surface morphology and MW of the reactor powder. The smooth surface accelerates the adhesion between the powder particles within the prepared film, thus the high ductility of the reactor powder can be utilized to give the resultant higher DR_{max}. The higher MW means the fewer mounts of the chain ends within the film, leading to the higher tensile strength. In this study, the highest E_{max} of ~25 GPa was finally achieved, which corresponds to 70% of the theoretical modulus of iPP crystal. The σ_{max} of ~1.0 GPa is three times as high as those of commercial high-strength iPP tapes. Further, it is reasonable to be thought that the remaining less-entangled state of reactor powder within the direct-calendared film is a key for achieving the resultant high performances.

It is widely recognized that the iPP is more degradable than PE with melt-extrusion; thus, the additives such as antioxidants are added in industries. If the reactor powder processing examined in this study is applied, such melt-extrusion process can be skipped, and thus additive-free processing into the high-performance iPP film becomes possible. This processing technique is expected to extend such processing with less environmental loading.

4. Conclusions

Two UHMW-iPP reactor powders synthesized using the same Ziegler–Natta catalyst system were directly calendar-rolled into the film below their T_m with skipping the conventional melt-extrusion processes. The prepared film was successfully ultra drawn by tensile force and the resultant film exhibited the high modulus and strength. A combination of DSC and WAXD measurements revealed that the oriented crystallization occurred during tensile drawing. The resultant mechanical properties increased with increasing DR, due to such crystallinity development. The maximum tensile modulus achieved was ~25 GPa for the films prepared from an UHMW-iPP reactor powder having an M_w of 1.5×10^6. This value corresponds to 75% of the theoretical modulus of iPP crystal. The tensile strength of this ultra-drawn film was ~0.7 GPa. For the other reactor powder having an M_w of 2.3×10^6, the maximum tensile modulus was similar but a much higher strength of ~1.0 GPa was obtained. This strength value is three times higher than that of the commercial high-strength PP tape. Such a high processability of iPP reactor powder indicates that the as-polymerized morphology is composed of the highly crystalline state with less entanglement, as well as PE reactor powder. Direct film processing from reactor powder successfully remains the initial less-entangled state formed during polymerization. A comparison of the results obtained for modified iPP reactor powders exhibited that the surface flatness dominates the ultra-drawability and resultant properties of the reactor powder film.

Table 5
Maximum draw ratio ($DR_{t,max}$), tensile modulus (E_{max}) and strength (σ_{max}) for the film prepared from PP-2 reactor powder

Sample	$DR_{t,max}$	E_{max} (GPa)	σ_{max} (GPa)
PP-2	28	25 ± 1	1.0 ± 0.1

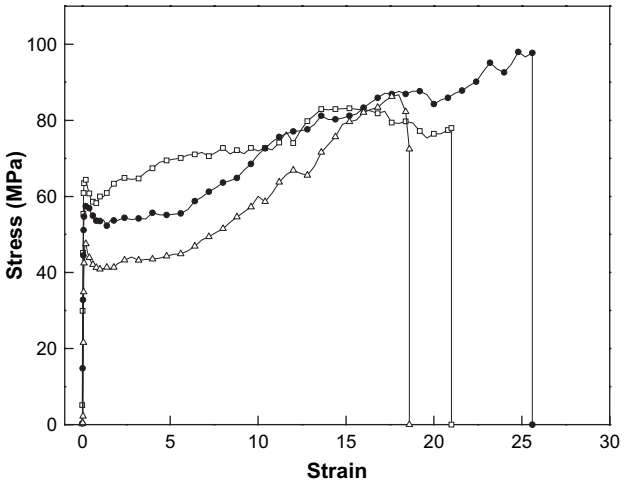

Fig. 11. Stress–strain curves recorded during drawing for the PP-2 film prepared at a T_{roll} of 165 °C. Draws were made at different T^1_{draw}s of 140 °C (□), 145 °C (●), and 150 °C (△).

Acknowledgments

This work was partly supported by Industrial Technology Research Grant Program in 2004 from the New Energy and Industrial Technology Development Organization (NEDO) of Japan.

References

[1] Bastiaansen CWM, Meyer HEH, Lemstra PJ. Polymer 1990;31:1435.
[2] Uehara H, Nakae M, Kanamoto T, Ohtsu O, Sano A, Matsuura K. Polymer 1998;39:6127.
[3] Uehara H, Yamanobe T, Komoto T. Macromolecules 2000;33:4861.
[4] Uehara H, Aoike T, Yamanobe T, Komoto T. Macromolecules 2002; 35:2640.
[5] Tsobkallo K, Vasilieva V, Khizhnyak S, Pakhomov P, Galitsyn V, Ruhl E, et al. Polymer 2003;44:1613.
[6] Rahl FJ, Evanco MA, Fredericks RJ, Reimschuessel AC. J Polym Sci Part A2 1972;10:1337.
[7] Folda T, Hoffmann H, Chanzy H, Smith P. Nature 1988;333:55.
[8] Kanamoto T, Ohama T, Tanaka K, Takeda M, Porter RS. Polymer 1987; 28:1517.
[9] Rotzinger BP, Chanzy HD, Smith P. Polymer 1989;30:1814.

[10] Wang LH, Ottani S, Porter RS. Polymer 1991;32:1776.
[11] Porter RS, Kanamoto T, Zachariades AE. Polymer 1994;35:4979.
[12] Uehara H, Kanamoto T, Kawaguchi A, Murakami S. Macromolecules 1996;29:1540.
[13] Nagai M, Uehara H, Kanamoto T. Koubunshi Ronbunsyu 1996;53:555.
[14] Uehara H, Jounai K, Endo R, Okuyama H, Kanamoto T, Porter RS. Polym J 1997;29:198.
[15] Endo R, Jounai K, Uehara H, Kanamoto T, Porter RS. J Polym Sci Polym Phys Ed 1998;36:2551.
[16] Karian HG. Handbook of polypropylene and polypropylene composites. New York: Marcel Dekker; 1999.
[17] Sakurada I, Kaji K. J Polym Sci Part C 1970;31:57.
[18] Kanamoto T, Tsuruta A, Tanaka K, Takeda M. Polym J 1984;16:75.
[19] Kakugo M, Sadatoshi M, Yokokawa M, Kojima K. Macromolecules 1989;22:547.
[20] Kakugo M, Sadatoshi H, Sakai J, Yokoyama M. Macromolecules 1989; 22:3172.
[21] Bailly JC, Hagege R. Polymer 1991;32:181.
[22] Noristi L, Marchetti E, Baruzzi G, Sgarzi P. J Polym Sci Polym Chem Ed 1994;32:3047.
[23] Zechlin J, Hauschild K, Fink G. Macromol Chem Phys 2000;201:515.
[24] Zechlin J, Hauschild K, Fink G. Macromol Chem Phys 2000;201:597.
[25] Wunderlich B. Macromolecular physics. In: Crystal structure, morphology, defects, vol. 1. New York: Academic Press; 1973.
[26] Garton A, Stepaniak RF, Carlsson DJ, Wiles DM. J Polym Sci Polym Phys Ed 1978;16:599.